animals

MDPI

Article

The Characterization and Differential Analysis of m^{6}A Methylation in Hycole Rabbit Muscle and Adipose Tissue and Prediction of Regulatory Mechanism about Intramuscular Fat

Gang Luo †, Yaotian Ai †, Lin Yu, Shuhui Wang and Zhanjun Ren *

College of Animal Science and Technology, Northwest A&F University, Xianyang 712100, China
* Correspondence: renzhanjun@nwsuaf.edu.cn
† These authors contributed equally to this work.

Simple Summary: At present, one of the main problems hindering the development of rabbit industry is the low intramuscular fat of rabbits. N6-methyladenosine (m^{6}A) is a highly dynamic RNA modification, which plays an important regulatory role in various physiological processes of animals. Sequencing rabbit longissimus lumborum muscle and perirenal fat by MeRIP-seq (methylated RNA immunoprecipitation with next-generation sequencing), we provided key prediction pathway for producing rabbit meat with good taste.

Abstract: N6-methyladenosine (m^{6}A) widely participates in various life processes of animals, including disease, memory, growth and development, etc. However, there is no report on m^{6}A regulating intramuscular fat deposition in rabbits. In this study, m^{6}A modification of Hycole rabbit muscle and adipose tissues were detected by MeRIP-Seq. In this case, 3 methylases and 12 genes modified by m^{6}A were found to be significantly different between muscle and adipose tissues. At the same time, we found 3 methylases can regulate the expression of 12 genes in different ways and the function of 12 genes is related to fat deposition base on existing studies. 12 genes were modified by m^{6}A methylase in rabbit muscle and adipose tissues. These results suggest that 3 methylases may regulate the expression of 12 genes through different pathways. In addition, the analysis of results showed that 6 of the 12 genes regulated eight signaling pathways, which regulated intramuscular fat deposition. RT-qPCR was used to validate the sequencing results and found the expression results of RT-qPCR and sequencing results are consistent. In summary, *METTL4*, *ZC3H13* and *IGF2BP2* regulated intramuscular fat by m^{6}A modified gene/signaling pathways. Our work provided a new molecular basis and a new way to produce rabbit meat with good taste.

Keywords: Hycole rabbit; m^{6}A; gene expression; methylase; intramuscula fat

check for updates

Citation: Luo, G.; Ai, Y.; Yu, L.; Wang, S.; Ren, Z. The Characterization and Differential Analysis of m^{6}A Methylation in Hycole Rabbit Muscle and Adipose Tissue and Prediction of Regulatory Mechanism about Intramuscular Fat. *Animals* **2023**, *13*, 446. https://doi.org/10.3390/ani13030446

Academic Editor: Ioanna-Katerina Aggeli

Received: 27 November 2022
Revised: 24 January 2023
Accepted: 25 January 2023
Published: 28 January 2023

Copyright: © 2023 by the authors. Licensee MDPI, Basel, Switzerland. This article is an open access article distributed under the terms and conditions of the Creative Commons Attribution (CC BY) license (https://creativecommons.org/licenses/by/4.0/).

1. Introduction

N6-methyladenosine (m^{6}A) is the most common internal modification form of mRNA in eukaryotes [1], which affects a variety of biological processes, including splicing, processing, translation, stability and decay, nuclear export, cellular metabolism and differentiation [2,3]. M^{6}A is mainly regulated by methylase [4–8] (*ZC3H13*, *METTL4*, *KIAA1492*, *WTAP*, *METTL14*, *RBM15/15B*, *METTL3*), demethylase [9,10] (ALKBH5, FTO) and recognition enzyme (*IGF2BP2*, *YTHDF1-3*, *HNRNPA2B1*, *YTHDC1-2*) [11–13]. M^{6}A modification is widely distributed in animal tissues such as lung, brain, kidney, liver, and heart, and exhibits tissue-specific regulation [6,14].

METTL4 mediated m^{6}A methylation based on a past phylogenetic prediction of N6-methylation [15–17]. Knockdown of *METTL4* led to the change of adipocyte differentiation, shown by defective gene regulation and impaired lipid production [8]. *ZC3H13* is critical for mRNA m^{6}A methylation [7]. Upstream of NF-κB may be activated by *ZC3H13* [18] and NF-κB signaling plays an important role in adipocyte differentiation [19]. Studies showed

IGF2BP2 is a m^{6}A methylated reading protein [20]. In addition, *IGF2BP2* is a growth factor that plays a key role in regulating the translation of *IGF2* and controls fetal growth and organ formation, including adipogenesis and pancreatic development [21]. However, the specific mechanism of *METTL4*, *ZC3H13* and *IGF2BP2* regulating fat deposition through m^{6}A modification is unclear.

With the development of society, obesity has become a more and more serious health problem for contemporary people [22]. In addition, Adipose tissues plays an important role not only in heat generation and lipid storage, but also in muscle flavor. Adipose tissues deposition at the cellular level is mainly reflected by the proliferation and differentiation of adipocytes. It is generally accepted that adipocyte differentiation and proliferation are highly regulated process that involves several transcription factors and modification modes. Studies have shown that *FABP3* [23], *COL6A5* [24], *FAM13A* [25], *MYOZ2* [26,27], *EGR2* [28], *SOX9* [29], *IRX5* [30], *PRKAG 3* [31], *ABCA1* [32], *ADRB1* [33], *ADAMTS18* [34,35] and *GLI2* [36,37] are important factors in the regulation of fat deposition. M^{6}A is involved in a variety of biological processes and the occurrence of a variety of diseases, including tumor, obesity and infertility [38]. Thus, it is of great value to unravel the mechanisms by which m^{6}A orchestrate adipocyte differentiation and proliferation by regulatory factors.

Intramuscular fat refers to the content of fat in muscle, and the longest dorsal muscle is the main component of rabbit meat. Perirenal fat is one of the adipose tissues closest to the longest dorsal muscle, and also the main white fat that can be collected from 0-day-old rabbits. In this study, we used newborn rabbits to study the regulation of m^{6}A on muscle and adipose tissues development through MeRIP-seq sequencing. Subsequently, we mapped the m^{6}A map of transcriptome width of meat rabbits base on sequencing results. In addition, 3 differential methylases and 12 differential genes modified by m^{6}A related to fat deposition between muscle and adipose tissues were found. 3 differential methylases regulated the expression of 12 differential genes modified by m^{6}A in different ways. In addition, 6 of the 12 genes regulated eight signaling pathways, which regulate intramuscular fat deposition. The study has laid a molecular theoretical foundation for cultivating excellent rabbits.

2. Material and Methods

2.1. Ethics Statement

All experimental procedures were reviewed and approved by the Institutional Animal Care and Use Committee (IACUC) of Northwest A&F University, under the permit No. DK 2022045.

2.2. Animals and Tissues Collection

We collected the perirenal fat and the longissimus lumborum of 3 female Hycole rabbits. They were 0 days old and had the same environment. After rabbits were humanely sacrificed to ameliorate suffering, the longissimus lumborum and perirenal adipose tissues of rabbits were quickly separated. Subsequently, we placed the sample in the −80 °C refrigerator after quick freezing with liquid nitrogen.

2.3. RNA Extraction and Fragmentation

Total RNA was got by using Trizol reagent (Fankewei, Xianyang, China). We used Dynabeads® mRNA purification kit (Ambion, Texas, USA) for purification after RNA detection. All of the purified mRNA was randomly broken into ∼100 nt fragments by Magnesium RNA Fragmentation Module (NEB, Beijing, China) for the construction of a MeRIP-Seq (methylated RNA immunoprecipitation and sequencing) library.

2.4. M^{6}A Immunoprecipitation and Library Construction

The fragmented mRNA was divided into two parts, one of which used for immunoprecipitation (IP) based on the method used by Dominissini et al. [14]. The cleaved RNA fragments were combined with antibody, then reverse transcribed into cDNA. The blunt

ends were connected to an A-base for ligation to the indexed adapters. After size selection, we used the heat-labile UDG enzyme (Baltimore, MD, USA) to treat the U-labeled second-stranded DNA and amplified the ligated products with PCR. Finally, we performed the 2 × 150 bp paired-end sequencing on an illumina Novaseq™ 6000 (Lianchuan, Hangzhou, China). The specific method used is the same as that of Wang et al. [39].

2.5. MeRIP-Seq

After cDNA synthesis, end repair, the addition of an A tail and connectors, cDNA fragment purification, and PCR enrichment of fragmented mRNA, we performed the 2 × 150 bp paired-end sequencing (PE150) on an illumina Novaseq™ 6000 (LC-Bio Technology CO., Ltd., Hangzhou, China) following the vendor's recommended protocol.

2.6. RT-qPCR

Primers were designed with premier 6 software (http://www.greenxf.com/soft/190969.html (accessed on 18 January 2018)) (6.1, Premier company, Canada). Primer sequences are in Table 1. After synthesizing cDNA, we used SYBR Green [40] to conduct RT-qPCR. With β-actin as the internal reference, we use the $2^{-\Delta\Delta Ct}$ method to analyze the results.

Table 1. Primers used in this study.

Gene Name	Primer Sequence (5′→3′)	(Tm/°C)
β-actin	GGAGATCGTGCGGGACAT GTTGAAGGTGGTCTCGTGGAT	61.4
ADRB1	CATCATCATGGGCGTGTTCA TAGCCGAGCCAGTTGAAGAA	51.8

2.7. Quality Control, Mapping and Statistical Analysis

Firstly, we used fastp software [41] to control the quality of raw reads(Remove reads that contain more than 5% of N), filtered the low-quality data (Alkali base with mass value $Q \leq 10$ accounts for more than 20% of the total read) and acquire clean reads (Sequencing error rate is less than 0.01). Next, we used bowtie2 [42] to compare the high quality clean reads to the ribosomal database of the species and removed the reads of ribosomal RNA on the comparison. Comparison of reference genomes using software HISAT2 (http://daehwankimlab.github.io/hisat2) (accessed on 24 July 2020). (JOHNS HOPKINS University, Homewood, US). We made detailed statistics on the comparison of sequencing data, and evaluated the selection of reference sequences and the comparison results of sequencing data. The main analysis software of TF-motif analysis is MEME (http://meme-suite.org) (accessed on 3 September 2015) (UC San Diego, California, US) and peak between groups were analyzed by DiffBind [43]. The number of peak-related genes of GO function is to transfer peak-related genes to GO database (http://www.geneontology.org/ (accessed on 26 November 2022)) and calculate the number of peak-related genes of each term. With KEGG Pathway as the unit, hypergeometric test is applied to find out the Pathway that is significantly enriched in peak-related genes in the whole genome background. The most important biochemical metabolic pathway and signal transduction pathway involved in peak-related genes were determined through the significant enrichment of Pathway. GraphPad Prism7 (University Of California, State of California, US) was used to detect RT-qPCR and draw figures. We used two-tail Student's t-test to analyze the significance of the different levels. The standards of significant and extremely significant are $p < 0.05$ and $p < 0.01$, respectively.

3. Results

3.1. Data Filtering and Quality Evaluation

Clean reads were obtained after removing low quality data and filtering the original data. As shown in Figure 1A,B, the sequencing data of muscle and fat are completely up to

standard after processing. Cluster analysis showed that muscle and adipose tissues were significantly clustered, respectively (Figure 1C). In addition, we found that low-quality data in all organizations accounted for less than 7% of all data (including Q20% and q30%) (Table S1). The proportion of base GC is greater than 50% after filtration (Table S1). By comparing reads with reference sequences, we found unique mapped reads of all samples were more than 50% (Table S2).

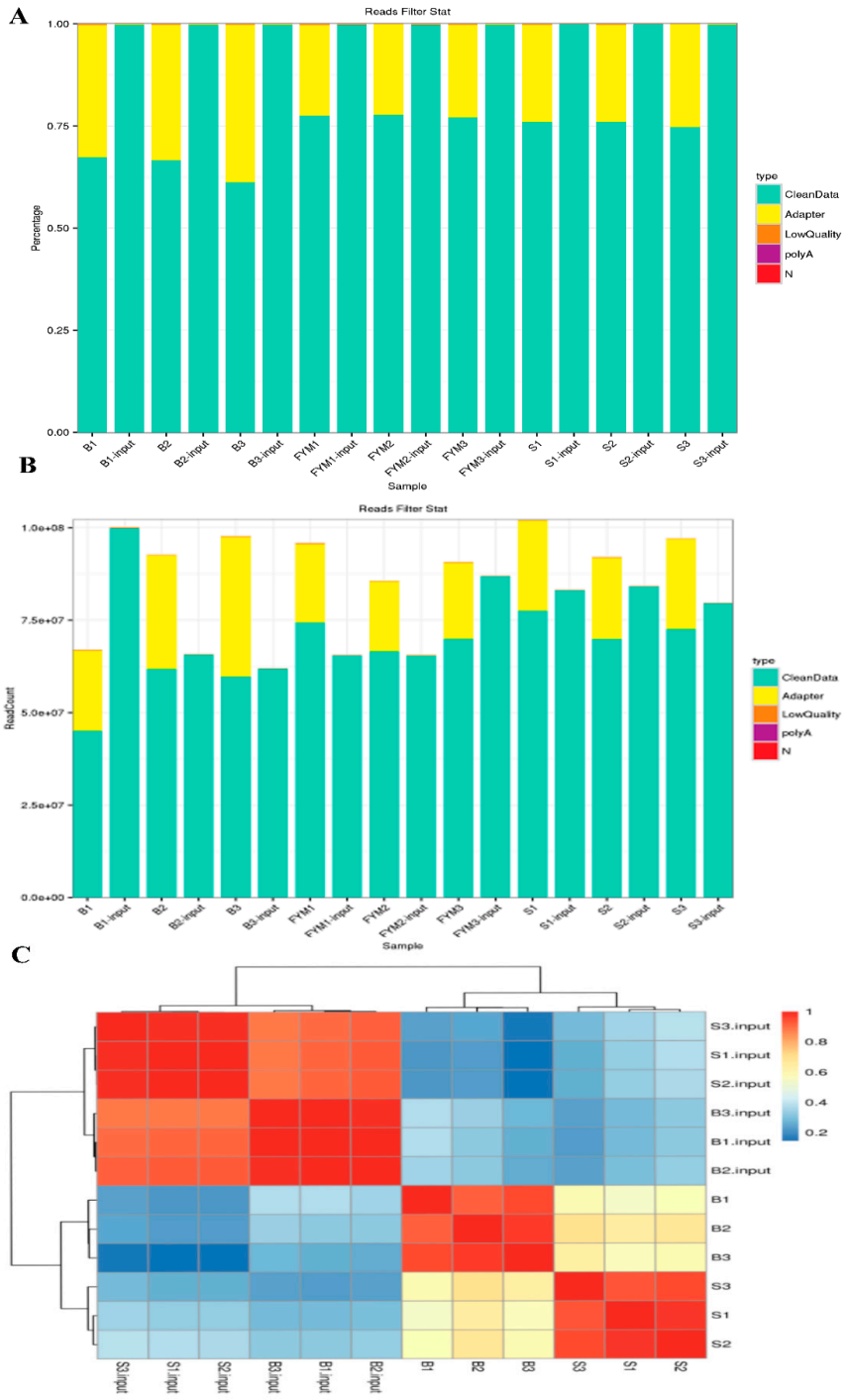

Figure 1. Data processing and sample clustering; (**A**) Data preprocessing distribution (percentage); (**B**) Data preprocessing distribution(value); (**C**) Clustering of muscle and fat samples. ('B' refers to the longest dorsal muscle and 'S' refers to perirenal fat).

3.2. General Features of Rabbit m^{6}A Methylation

The results showed that GACGGTG and GTCCATG were significantly enriched in muscle tissues and adipose tissue, which conforms the conservative sequence RRACH motif in the m^{6}A peaks (Figure 2A). In addition, we found that the peaks located in the CDS and the start codons regions of muscle were more abundant than that in fat tissues whereas peaks in start codon segment and 3′UTR are more abundant in adipose tissues (Figure 2B,C). As shown in Table 2, we found 6971 peaks in muscle with an average length of 1118 bp and 7028 peaks in adipose tissues with an average length of 1117 bp. However, the genome rate of muscle tissues is less than that of adipose tissue.

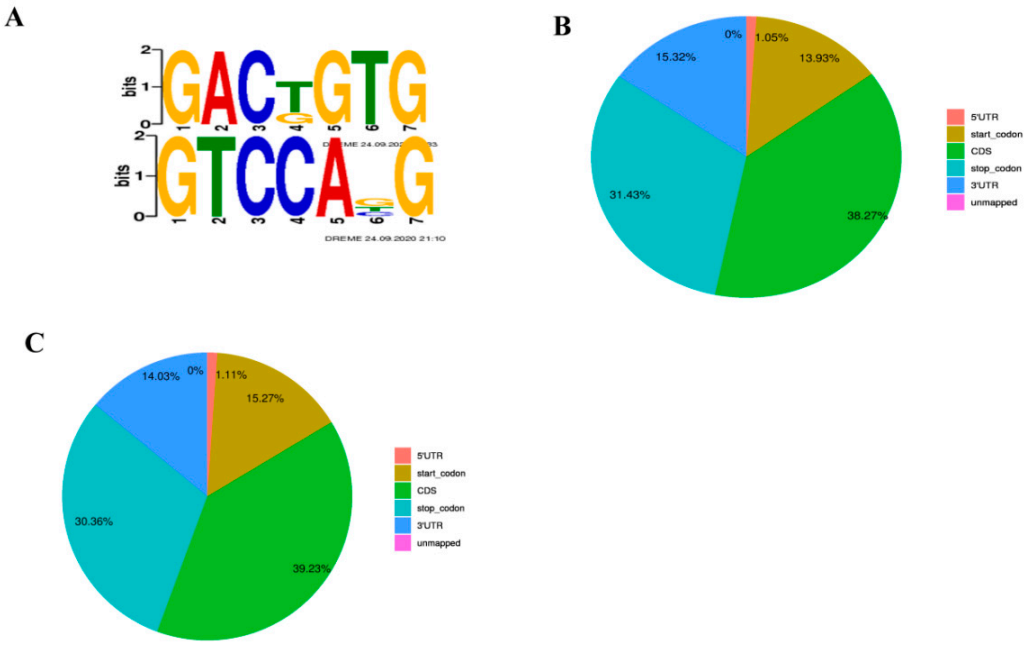

Figure 2. Summary of peaks (**A**) Motif sequence diagram; (**B**) Distribution of peaks in adipose tissue; (**C**) Distribution of peaks in muscle tissue. ('B' refers to the longest dorsal muscle and 'S' refers to perirenal fat).

Table 2. Summary of peaks.

Sample	Peak Number	Total Length	Average Length	Genome Rate (%)
B	6971	7800148	1118	0.347
S	7028	8055673	1117	0.358

Note: 'B' refers to the longest dorsal muscle and 'S' refers to perirenal fat.

3.3. Unique Features of Rabbit m^{6}A Methylation

In this case, 5280 m^{6}A peaks were in muscle and fat tissues. At the same time, we detected 1691 and 1928 peaks were specifically methylated in muscle and adipose tissues, respectively (Figure 3A). 230 peaks in muscle tissues were up-regulated and 101 peaks were down regulated compared with adipose tissues (Figure 3B). After annotating the inter group difference peak related genes, we found that 242 differential genes in muscle tissues were up-regulated and 120 differential genes were down regulated relative to adipose tissues (Figure 3C).

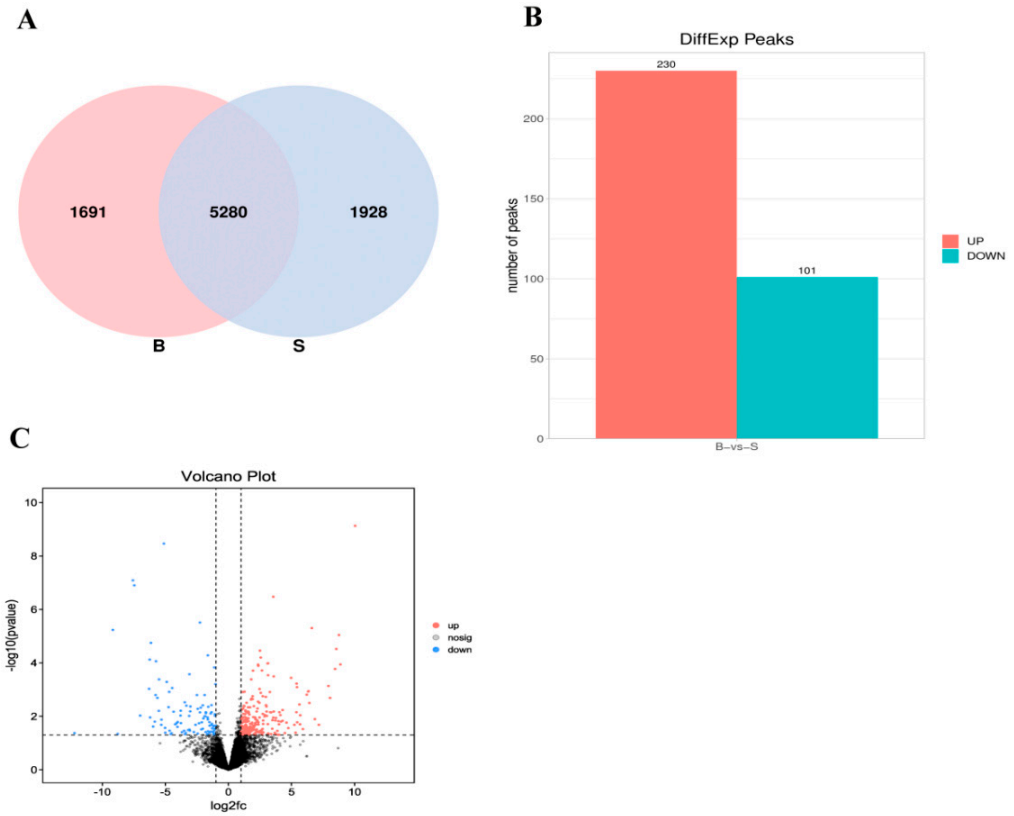

Figure 3. Peak analysis of difference between groups; (**A**) Common and unique peak of adipose and muscle tissue; (**B**) Difference peak histogram; (**C**) Analysis of peak related genes between adipose and muscle tissue. ('B' refers to the longest dorsal muscle and 'S' refers to perirenal fat).

3.4. GO Analysis and KEGG Pathway Analysis of Differently Methylated Genes

The results of enrichment analysis showed that peaks related genes in adipose tissues and muscle tissues mainly regulated the processes of biological process(cellular process, response to stimulus, biological regulation, regulation of biological process, metabolic process, multicellular organismal process, positive regulation of biological process, cellular component organization or biogenesis, developmental process, signaling, localization, negative regulation of biological process), cellular component(cell, membrane part, cell part, organelle, protein containing complex, organelle part, membrane-enclosed lumen) and molecular function(binding, catalytic activity) (Figure 4A,B). In addition, peaks related genes of adipose tissues were more than those of muscle tissues in the processes of biological process, cellular component and molecular function. To predict the functions of the m^6A-modified genes associated with fat deposition, we conducted KEGG pathway analysis. We found that the genes related to peaks mainly appeared in MAPK signaling pathway, Hippo signaling pathway, Notch signaling pathway, Wnt signaling pathway, mTOR signaling pathway, AMPK signaling pathway, cAMP signaling pathway, Adipocytokine signaling pathway, Regulation of lipolysis in adipocyte, Fatty acid metabolism and Non-alcoholic fatty liver disease pathways (Figure 5). Finally, we found that genes of signaling pathways related to fat deposition are more in adipose tissues than those in muscle tissues except MAPK signaling pathway (Figure 5).

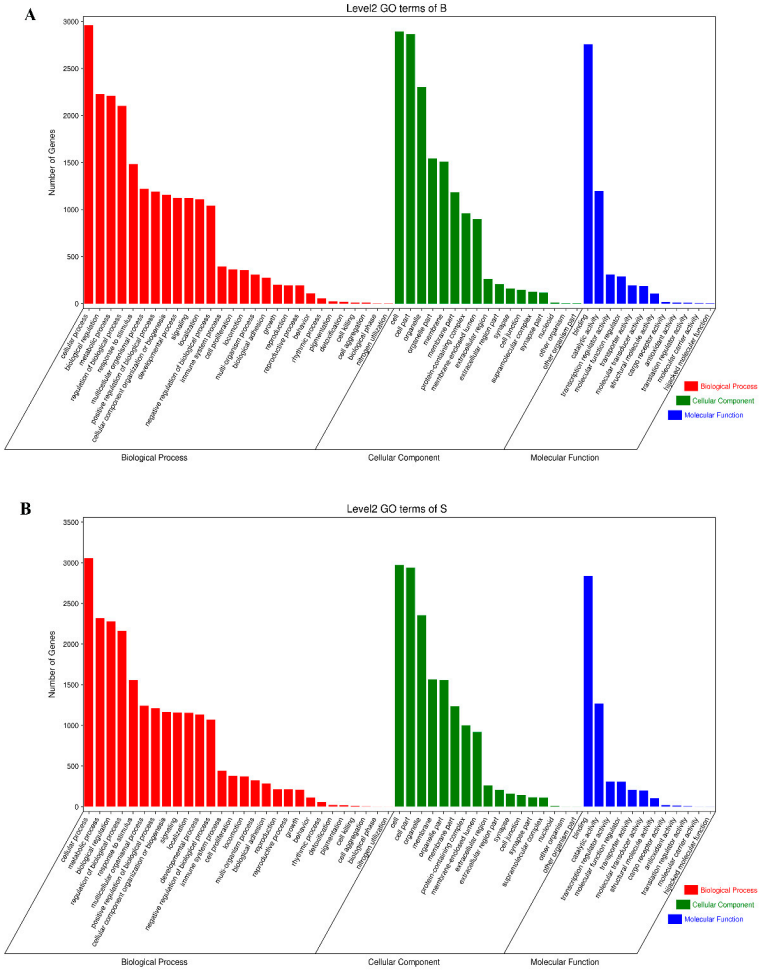

Figure 4. Go enrichment analysis of differential peak related genes; (**A**) Go enrichment classification histogram of muscle tissue; (**B**) Go enrichment classification histogram of fat tissue.

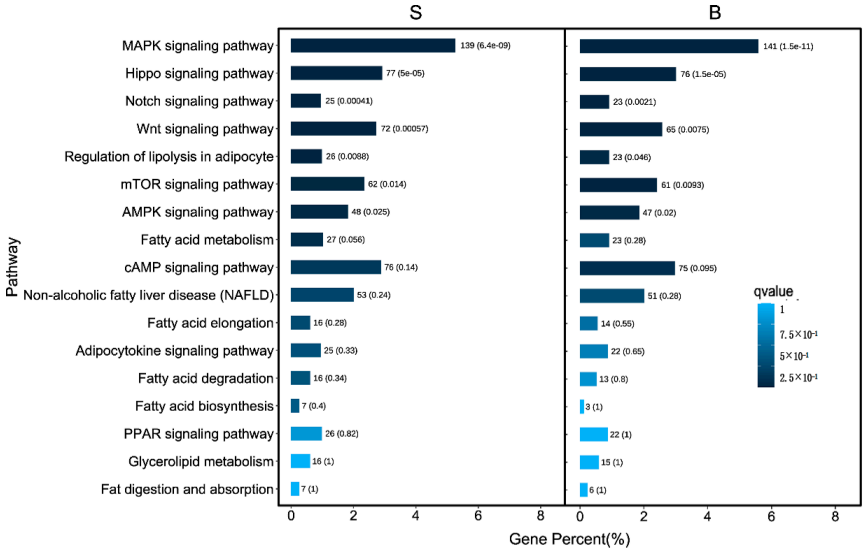

Figure 5. Enrichment analysis of fat metabolism related pathway KEGG. ('B' refers to the longest dorsal muscle and 'S' refers to perirenal fat). Note: The pathway is the vertical coordinate, the number of all peak-related genes are indicated on the horizontal coordinate.

3.5. Difference Analysis of Methylase and m^{6}A Modified Genes between Muscle and Adipose Tissue

We identified and screened three methylases between fat and muscle tissues. As shown in Table 3, *ZC3H13*, *METTL4* and *IGF2BP2* are distributed on chromosomes 8, 9 and 14, respectively. In addition, we found 49156464 to 49163130 bp of *ZC3H13*, 59497322 to 59497522 bp of *METTL4* and 79807766 to 79979443 bp of *IGF2BP2* are modified with m^{6}A. After analyzing and calculating the rpm value of methylase in the sequencing results, we found the expression levels of *METTL4* and *ZC3H13* in adipose tissues were significantly higher than those in muscle tissues whereas the expression of *IGF2BP2* in muscle tissues was significantly higher than that in adipose tissues (Figure 6A). Based on gene function, we found 12 differential expression genes associated with fat deposition between muscle and adipose tissues (Table 4). The distribution of genes on chromosomes, the location of m^{6}A modified genes and their expression differences are shown in Table 4. In addition, we found the expression levels of *ABCA1*, *ADRB1* and *ADAMTS18* in adipose tissues were significantly higher than those in muscle tissues whereas the expression levels of *FABP3*, *COL6A5*, *FAM13A*, *MYOZ2*, *EGR2*, *SOX9*, *IRX5*, *PRKAG3* and *GLI2* in adipose tissues were significantly lower than those in muscle tissues (Figure 6B). To verify the sequencing results, we selected *ADRB1* gene for RT-qPCR and found *ADRB1* expression level was in adipose tissues was significantly higher than that in muscle tissues (Figure 6C).

Table 3. Summary of methylase genes between muscle and fat tissues.

Symbol	Chromosome	Start	End	Gene_Start	Gene_End
ZC3H13	8	49156464	49163130	49112198	49203390
METTL4	9	59497322	59497522	59489716	59522894
IGF2BP2	14	79807766	79979443	79807317	79979658

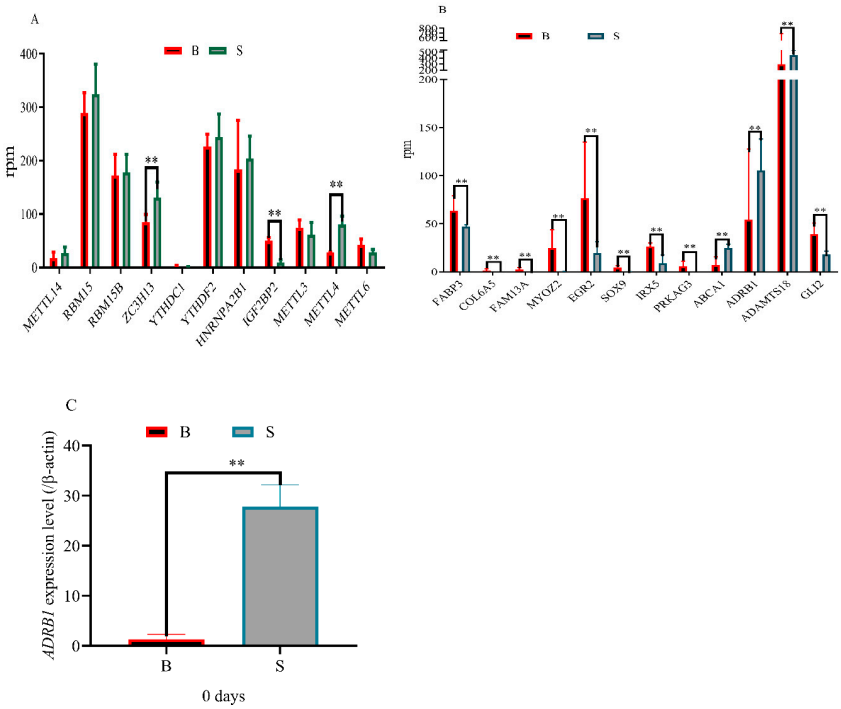

Figure 6. Overview of differentially expressed of methylase genes and key genes in muscle and adipose tissues samples (**A**) RPM of the methylase genes in muscle and adipose tissues; (**B**) RPM of the key genes in muscle and adipose tissues; (**C**) Expression level of *ADRB1* gene in muscle and adipose tissues ($p < 0.01$). ('B' refers to the longest dorsal muscle and 'S' refers to perirenal fat) ("**", $p \leq 0.01$).

Table 4. Difference analysis of fat related genes between muscle and fat tissues.

Symbol	Chromosome	Gene_Start	Gene_End	Diff.log2FC	*p*-Value
ABCA1	1	8128276	8262632	1.258322149	0.030511101
IRX5	5	11211307	11214739	3.145191738	0.043951603
ADAMTS18	5	31919264	32078296	1.763515547	0.026105306
GLI2	7	59796306	59899847	2.106650174	0.018530687
PRKAG3	7	160092580	160099205	−3.456695972	0.047136086
FABP3	13	134849947	134860535	−1.076952166	0.008346079
COL6A5	14	963915	1100656	−7.002296213	0.009463418
FAM13A	15	60958616	61325685	−5.001719634	0.041259027
MYOZ2	15	94465177	94502456	3.759079992	0.011579319
EGR2	18	23380925	23387584	1.671242666	0.03208062
ADRB1	18	61629975	61631390	5.667263578	0.020071817
SOX9	19	55820444	55823755	−5.772627603	0.001606224

3.6. Regulation of Methylase on the Expression of m^{6}A Modifying Genes Related to Fat Deposition

As shown in Figure 7, we found *ZC3H13* regulated expression levels of *FAM13A*, *MYOZ2* and *ADAMTS18* genes through *NF-KB*. *METTL4* regulated expression levels of *GLI2*, *COL6A5*, *SOX9*, *FABP3* and *PRKAG3* genes through *AKT* gene. *IGF2BP2* regulated expression levels of *ABCA1*, *ADRB1*, *ADAMTS18*, *FABP3*, *COL6A5*, *FAM13A*, *MYOZ2*, *EGR2*, *SOX9*, *IRX5*, *PRKAG3* and *GLI2* genes through multiple pathways.

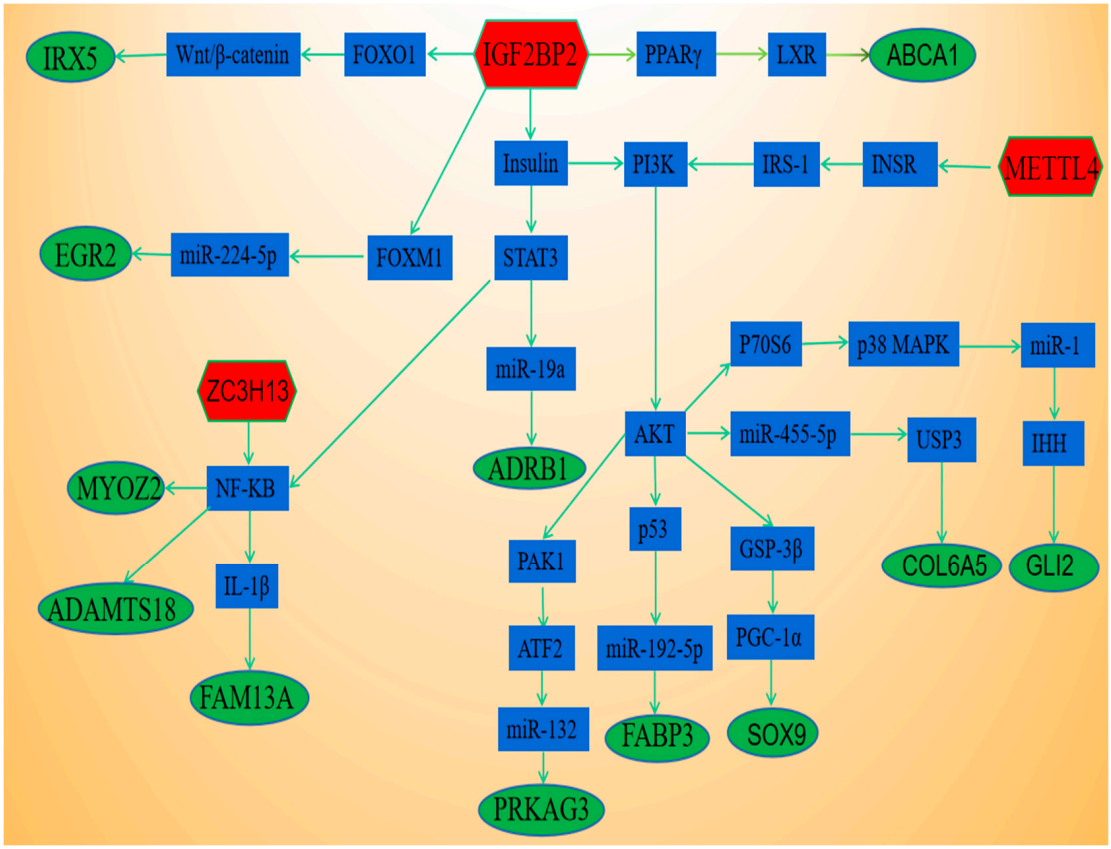

Figure 7. Regulation of fat related genes by methylase.

3.7. Methylase Regulated Genes Related to Fat Deposition through Signal Pathway

In order to explore the connection between m^{6}A modifying genes related to fat deposition and signaling pathways, we made Sankey diagram and found that 6 genes regulated 8 signaling pathways by multiple pathways (Figure 8). *SOX9*, *GLI2*, *FABP3* and *ABCA1* can regulate cAMP, Hippo, PPAR and Fat digestion and absorption signaling pathways,

respectively. *ADRB1* is involved in the regulation of cAMP and regulation of lipolysis in adipocyte signaling pathways. In addition, PPKAG3 play important roles in Adipocytokine signaling pathway, AMPK signaling pathway and Non-alcoholic fatty liver disease (NAFLD) signaling pathway (Figure 8).

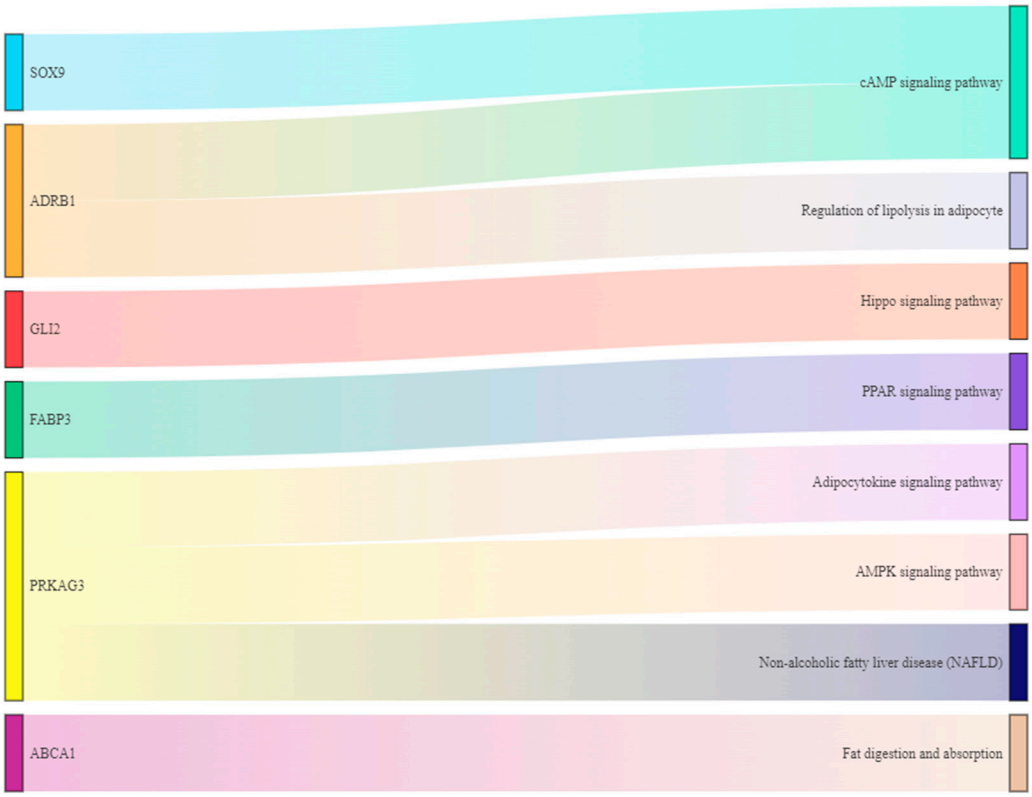

Figure 8. Association between genes and signaling pathways.

4. Discussion

Adipose tissues can regulate energy storage and energy metabolism [44,45]. In addition, adipose tissues are the main component of intramuscular fat and intramuscular fat is the main factor affecting meat quality and flavor. Studies have shown that m^6A plays an important role in the regulation of fat deposition. Therefore, we explored the regulatory mechanism of m^6A on intramuscular fat deposition by MeRIP-seq sequencing of rabbit muscle and adipose tissues.

In this study, we discovered that rabbit mRNA m^6A sites are mainly enriched around stop codons, CDS, and 3′UTRs by using MeRIP-Seq technology, which shared a distribution similar to that of pigs [46]. "RRACH" has been confirmed as the specific sequence of m^6A motif by multiple sequencing [14,47–49]. However, "RRACH" sequence appeared in large numbers in our current data, which indicated the transcriptome of rabbits have multiple m^6A modification sites. In addition, GO and KEGG pathway analysis were performed to deduce function on fat deposition of m^6A modified genes. After GO enrichment analysis, the differential peaks related genes are mainly distributed in biological process (cellular process, biological regulation, metabolic process, regulation of biological process, response to stimulus, multicellular organismal process, positive regulation of biological process, cellular component organization or biogenesis, developmental process, signaling, localization, negative regulation of biological process), which are the main process of fat deposition (Figure 4). The results of KEGG pathway analysis showed main signal pathways play a vital role in the regulation of fat deposition, such as MAPK signaling pathway [50], Hippo signaling pathway [51], Notch signaling pathway [52], Wnt signaling pathway [53], mTOR signaling pathway [54], AMPK signaling pathway [55], cAMP signal-

ing pathway [56], Adipocytokine signaling pathway, Regulation of lipolysis in adipocyte, Fatty acid metabolism and Non-alcoholic fatty liver disease pathways (Figure. 5). The results indicated that m^6A regulates fat deposition through multiple signaling pathways.

In the present study, the expression levels of *METTL4* and *ZC3H13* in adipose tissues were significantly higher than those in muscle tissues whereas the expression levels of *IGF2BP2* in adipose tissues was significantly lower than that in muscle tissues. The results are consistent with previous studies that *METTL4* [8] and *ZC3H13* [18,19] promoted fat production whereas *IGF2BP2* [21] inhibited fat production. Our results showed that several important lipogenic genes, including *ABCA1*, *ADRB1*, *ADAMTS18*, *FABP3*, *COL6A5*, *FAM13A*, *MYOZ2*, *EGR2*, *SOX9*, *IRX5*, *PRKAG3* and *GLI2* had variations in both m^6A methylation and mRNA expression. As an important part of fat deposition genetic network, *METTL4*, *ZC3H13* and *IGF2BP2* can regulate the expression levels of differential genes through multiple pathways. *IGF2BP2* inhibited *PID1* expression through the *DANCR*/*FOXO1* axis [57] and *FOXO1* played an important role in regulating Wnt/β-catenin signaling [58]. As the upstream target of *IRX5*, WNT/Rspo1/β-catenin regulates the expression of *IRX5* [59]. Secondly, *IGF2BP2* regulates macrophage phenotypic activation by stabilizing *PPARγ* [60]. A *PPARγ-LXR-ABCA1* pathway played an important role in cholesterol efflux and atherogenesis [61]. Next, *IGF2BP2* regulates the expression level of miR-224-5p through interacting m^6A/*FOXM1* manner [62,63]. *EGR2* is a target gene of miR-224-5p [64]. Finally, *IGF2BP2* affected first-phase insulin secretion during hyperglycemic clamps [65]. On the one hand, insulin can regulate the expression of *ADRB1* through *STAT3*/miR-19a pathway [66–68]. On the other hand, insulin stimulates translocation of *NF-kB* to the nucleus by activating a *PI3K*/*AKT*/*P70S6*/*p38-MAPK*/*MAPKAPK-2* cascade [69].

Another methylase *ZC3H13* is responsible for activating *NF-κB* [18]. Curcumin down-regulated *ADAMTS18* gene though *NF-κB* Signaling Pathway [70]. *NF-κB* can regulate the activity of *MYOZ2* gene [71]. In addition, *NF-κB* played critical roles in the regulation of *IL-1β* [72] and *IL-1β* in adipose tissues increased inhibition of *FAM13A* expression [73]. In addition, knockdown of *METTL4* led to decreased N6-adenine methylation at the promoter region of *INSR* gene, down-regulated gene expression, inactivated the *INSR* pathway, and promotes lipid production of adipocytes [8]. *INSR* regulates type 2 diabetic through *IRS-1*/*PI3K* pathway [74]. *PI3K* played an important role in protecting intestinal stem cells through the *AKT*/p53 axis [75]. *P53* activates miR-192-5p to mediate *FABP3* gene [76,77]. Second, *AKT* regulates cancer cells by *PAK1*/*ATF2*/miR-132 signaling axis [78,79] and *PRKAG3* is a target gene of miR-132 [80]. Third, *AKT* Regulates Mitochondrial Biogenesis by *GSK-3β*/*PGC-1α* Pathway [81] and *PGC-1α* directly interacts with *SOX9* and promotes *SOX9*-dependent transcriptional activity [82]. Fourth, *AKT* plays an important role in regulating miR-455-5p [83] and *USP3* is the target gene of miR-455-5p [84]. *USP3* regulates *COL9A3*/*COL6A5* stabilisation to promote gastric cancer progression [85]. Finally, *AKT* stimulates translocation of *NF-kB* to the nucleus by *P70S6*/*p38-MAPK*/*MAPKAPK-2* cascade [69] and *p38 MAPK* Signal Pathway can inhibit miR-1 expression [86]. MiR-1 can delay the progression of osteoarthritis by inhibiting *IHH* [87] and *IHH* regulates *RUNX2* through *GLI2* to stimulate osteoblast differentiation [88]. These results indicated *METTL4*, *ZC3H13* and *IGF2BP2* can regulate the expression of *ABCA1*, *ADRB1*, *ADAMTS18*, *FABP3*, *COL6A5*, *FAM13A*, *MYOZ2*, *EGR2*, *SOX9*, *IRX5*, *PRKAG3* and *GLI2* genes through multiple pathways.

The results of Sankey diagram show that 6 m^6A-modified genes regulated cAMP signaling pathway, Hippo signaling pathway, PPAR signaling pathway, Fat digestion and absorption signaling pathway, Regulation of lipolysis in adipocyte signaling pathways, Adipocytokine signaling pathway, AMPK signaling pathway and Non-alcoholic fatty liver disease (NAFLD) signaling pathway. Studies indicated cAMP regulates the fat deposition in adipose tissues of finishing pigs through PKA pathway regulates [89]. Hippo and PPAR signaling pathways regulate adipocyte differentiation [90,91]. AMPK suppresses the adipogenesis in human adipose derived stem cells [92]. Fat digestion and absorption signaling pathway, Regulation of lipolysis in adipocyte signaling pathways, Adipocytokine

signaling pathway and Non-alcoholic fatty liver disease (NAFLD) signaling pathway are classical signaling pathways regulating fat deposition in different tissues. These results indicated 8 signaling pathways can regulate fat deposition. At the same time, 8 signaling pathways are present in the muscle tissue. Therefore, cAMP signaling pathway, Hippo signaling pathway, PPAR signaling pathway, Fat digestion and absorption signaling pathway, Regulation of lipolysis in adipocyte signaling pathways, Adipocytokine signaling pathway, AMPK signaling pathway and Non-alcoholic fatty liver disease (NAFLD) signaling pathway are the main signal pathway regulating intramuscular fat. Although we have carried out a significant amount of work, there are still many deficiencies. In order to further explore the mechanism of intramuscular fat deposition, we will later verify these regulatory mechanisms in cells and in vivo to cultivate excellent rabbit breeds.

5. Conclusions

In summary, we revealed features of m^6A distribution in the Hycole rabbit perirenal fat and longissimus lumborum. Next, we screened 3 differential methylases and 12 genes modified by m^6A between muscle and adipose tissues. Based on the previous studies, we found that three methylases can regulate the expression of m^6A modified genes through different pathways. In addition, 6 of the 12 genes regulated eight signaling pathways, which regulated fat deposition in muscle tissue. These results indicated 3 differential methylases regulated intramuscular fat deposition via m^6A modifying gene/signaling pathways. This study provided a solid theoretical foundation and a new way to produce rabbit meat with good taste.

Supplementary Materials: The following supporting information can be downloaded at: https://www.mdpi.com/article/10.3390/ani13030446/s1, Table S1: Summary of reads quality control; Table S2: Summary of reads mapping to the rabbit reference genome.

Author Contributions: Conceptualization, Z.R. and G.L.; methodology, G.L.; software, G.L.; validation, G.L., L.Y. and Y.A.; formal analysis, Y.A.; data curation, Y.A.; writing—original draft preparation, G.L.; writing—review and editing, G.L.; supervision, S.W.; project administration, Y.A.; funding acquisition, Z.R. All authors have read and agreed to the published version of the manuscript.

Funding: This work was supported by Yangling Demonstration Area Industry University research and application collaborative innovation major project (1017cxy-15), Research, development, demonstration and promotion of key technologies for efficient and healthy rabbit breeding (K3360218032), Key technologies of large-scale and standardized healthy breeding of rabbits (K3370220034), Integrated promotion of technological innovation for improving quality and efficiency of rabbit industry (K3030821029) and Integration and demonstration of rabbit breeding and factory breeding technology (2018ZDXM-NY-041).

Institutional Review Board Statement: The animal use protocol has been reviewed and approved by the animal ethical and welfare committee, Northwest A&F University, China. Permit number is DK2022045.

Informed Consent Statement: Not applicable.

Data Availability Statement: Raw data can be obtained from NCBI database. The submission ID is SUB11353640 and BioProject ID is PRJNA830993.

Acknowledgments: We thank teachers and students of special economic animal health breeding research group, College of Animal Science and Technology, Northwest A&F University.

Conflicts of Interest: The authors declare no conflict of interest.

References

1. Wei, C.-M.; Gershowitz, A.; Moss, B. Methylated nucleotides block 5′ terminus of HeLa cell messenger RNA. *Cell* **1975**, *4*, 379–386. [CrossRef] [PubMed]
2. Shi, H.; Wang, X.; Lu, Z.; Zhao, B.S.; Ma, H.; Hsu, P.J.; Liu, C.; He, C. YTHDF3 facilitates translation and decay of N^6-methyladenosine-modified RNA. *Cell Res.* **2017**, *27*, 315–328. [CrossRef] [PubMed]
3. Wang, X.; He, C. Dynamic rna modifications in posttranscriptional regulation. *Mol. Cell* **2014**, *56*, 5–12. [CrossRef] [PubMed]

4. Liu, J.; Yue, Y.; Han, D.; Wang, X.; Fu, Y.; Zhang, L.; He, C.A. mettl3-mettl14 complex mediates mammalian nuclear rna n^6-adenosine methylation. *Nat. Chem. Biol.* **2014**, *10*, 93–95. [CrossRef]
5. Ping, X.-L.; Sun, B.-F.; Wang, L.; Xiao, W.; Yang, X.; Wang, W.-J.; Adhikari, S.; Shi, Y.; Lv, Y.; Chen, Y.-S.; et al. Mammalian WTAP is a regulatory subunit of the RNA N6-methyladenosine methyltransferase. *Cell Res.* **2014**, *24*, 177–189. [CrossRef]
6. Patil, D.P.; Chen, C.-K.; Pickering, B.F.; Chow, A.; Jackson, C.; Guttman, M.; Jaffrey, S.R. m6A RNA methylation promotes XIST-mediated transcriptional repression. *Nature* **2016**, *537*, 369–373. [CrossRef] [PubMed]
7. Wen, J.; Lv, R.; Ma, H.; Shen, H.; He, C.; Wang, J.; Jiao, F.; Liu, H.; Yang, P.; Tan, L.; et al. Zc3h13 Regulates Nuclear RNA m6A Methylation and Mouse Embryonic Stem Cell Self-Renewal. *Mol. Cell* **2018**, *69*, 1028–1038.e6. [CrossRef]
8. Zhang, Z.; Hou, Y.; Wang, Y.; Gao, T.; Ma, Z.; Yang, Y.; Zhang, P.; Yi, F.; Zhan, J.; Zhang, H.; et al. Regulation of Adipocyte Differentiation by METTL4, a 6 mA Methylase. *Sci. Rep.* **2020**, *10*, 8285. [CrossRef]
9. Jia, G.; Fu, Y.; Zhao, X.; Dai, Q.; Zheng, G.; Yang, Y.; Yi, C.; Lindahl, T.; Pan, T.; Yang, Y.-G.; et al. N6-Methyladenosine in nuclear RNA is a major substrate of the obesityassociated FTO. *Nat. Chem. Biol.* **2011**, *7*, 885–887. [CrossRef]
10. Zheng, G.; Dahl, J.A.; Niu, Y.; Fedorcsak, P.; Huang, C.M.; Li, C.J.; He, C. Alkbh5 is a mammalian rna demethylase that impacts rna metabolism and mouse fertility. *Mol. Cell* **2013**, *49*, 18–29.
11. Deng, X.; Su, R.; Weng, H.; Huang, H.; Li, Z.; Chen, J. Rna n6-methyladenosine modification in cancers: Cur-rent status and perspectives. *Cell Res.* **2018**, *28*, 507–517. [CrossRef] [PubMed]
12. Alarcón, C.R.; Goodarzi, H.; Lee, H.; Liu, X.; Tavazoie, S.; Tavazoie, S.F. HNRNPA2B1 Is a Mediator of m6A-Dependent Nuclear RNA Processing Events. *Cell* **2015**, *162*, 1299–1308. [CrossRef] [PubMed]
13. Wang, J.; Chen, L.; Qiang, P. The role of igf2bp2, an m6a reader gene, in human metabolic diseases and cancers. *Cancer Cell Int.* **2021**, *21*, 2280. [CrossRef] [PubMed]
14. Dominissini, D.; Moshitch-Moshkovitz, S.; Schwartz, S.; Salmon-Divon, M.; Ungar, L.; Osenberg, S.; Cesarkas, K.; Jacob-Hirsch, J.; Amariglio, N.; Kupiec, M.; et al. Topology of the human and mouse m6A RNA methylomes revealed by m6A-seq. *Nature* **2012**, *485*, 201–206. [CrossRef] [PubMed]
15. Bujnicki, J.M.; Feder, M.; Radlinska, M.; Blumenthal, R.M. Structure prediction and phylogenetic analysis of a functionally diverse family of proteins homologous to the mt-a70 subunit of the human mrna:M6a methyltransferase. *J. Mol. Evol.* **2002**, *55*, 431–444. [CrossRef]
16. Greer, E.L.; Blanco, M.A.; Lei, G.; Sendinc, E.; Yang, S. DNA methylation on n-adenine in *C. elegans*. *Cell* **2015**, *161*, 868–878. [CrossRef]
17. Kweon, S.-M.; Chen, Y.; Moon, E.; Kvederaviciutė, K.; Klimasauskas, S.; Feldman, D.E. An Adversarial DNA N6-Methyladenine-Sensor Network Preserves Polycomb Silencing. *Mol. Cell* **2019**, *74*, 1137–1148. [CrossRef]
18. Gewurz, B.E.; Towfic, F.; Mar, J.C.; Shinners, N.P.; Takasaki, K.; Zhao, B.; Cahir-McFarland, E.D.; Quackenbush, J.; Xavier, R.J.; Kieff, E. Genome-wide siRNA screen for mediators of NF-κB activation. *Proc. Natl. Acad. Sci. USA* **2012**, *109*, 2467–2472. [CrossRef]
19. Weidemann, A.; Lovas, A.; Rauch, A.; Andreas, N.; Maltzahn, J.V.; Riemann, M.; Weih, F. Classical and alternative nf-κb signaling cooperate in regulating adipocyte differentiation and function. *Int. J. Obes.* **2016**, *40*, 452–459. [CrossRef]
20. Maity, A.; Das, B. N6-methyladenosine modification in mrna: Machinery, function and implications for health and diseases. *Febs J.* **2016**, *283*, 1607–1630. [CrossRef]
21. Le, H.T.T.; Sorrell, A.M.; Siddle, K. Two isoforms of the mrna binding protein igf2bp2 are generated by alternative translational initiation. *PLoS ONE* **2012**, *7*, e33140. [CrossRef] [PubMed]
22. Stefan, N.; Schick, F.; Häring, H.U. Causes, characteristics, and consequences of metabolically unhealthy normal weight in humans. *Cell Metab.* **2017**, *26*, 292–300. [CrossRef]
23. Tyra, M.; Ropka-Molik, K. Effect of the fabp3 and lepr gene polymorphisms and expression levels on intramuscular fat (imf) content and fat cover degree in pigs. *Livest. Sci.* **2011**, *142*, 114–120. [CrossRef]
24. Sun, L.F.; Yang, Y.L.; Wang, M.Y.; Zhao, H.S.; Zhang, J.V. Inhibition of col6a5 improve lipid metabolism disorder in dihydrotestosterone-induced hyperandrogenic mice. *Front. Cell Dev. Biol.* **2021**, *9*, 669189. [CrossRef]
25. Fathzadeh, M.; Li, J.; Rao, A.; Cook, N.; Chennamsetty, I.; Seldin, M.; Zhou, X.; Sangwung, P.; Gloudemans, M.J.; Keller, M.; et al. FAM13A affects body fat distribution and adipocyte function. *Nat. Commun.* **2020**, *11*, 1465. [CrossRef] [PubMed]
26. Mingzhou, L.I.; Jinyong, W.; Li, Z.; Xuewei, L.I.; Surong, S.; Xiaokun, T.; Huasheng, X.; Qiang, L.I.; Lei, C.; Yujiao, G. Expression profiling analysis for genes related to meat quality and carcass traits during postnatal development of backfat in two pig breeds. *Sci. China C Life Sci.* **2008**, *51*, 718–733.
27. Frey, N.; Olson, E.N. Calsarcin-3, a Novel Skeletal Muscle-specific Member of the Calsarcin Family, Interacts with Multiple Z-disc Proteins. *J. Biol. Chem.* **2002**, *277*, 13998–14004. [CrossRef]
28. Chen, Z.; Torrens, J.I.; Anand, A.; Spiegelman, B.M.; Friedman, J.M. Krox20 stimulates adipogenesis via c/ebpbeta-dependent and independent mechanisms. *Cell Metab.* **2005**, *1*, 93–106. [CrossRef]
29. Gulyaeva, O.; Nguyen, H.; Sambeat, A.; Heydari, K.; Sul, H.S. Sox9-meis1 inactivation is required for adipogenesis, advancing pref-1+ to pdgfrα+ cells. *Cell Rep.* **2018**, *25*, 1002–1017. [CrossRef]
30. Bjune, J.I.; Haugen, C.; Gudbrandsen, O.; Nordbø, O.; Nielsen, H.J.; Våge, V.; Njølstad, P.R.; Sagen, J.V.; Dankel, S.N.; Mellgren, G. Irx5 regulates adipocyte amyloid precursor protein and mitochondrial respiration in obesity. *Int. J. Obes.* **2018**, *43*, 2151–2162. [CrossRef]

31. Zierath, B.R.B. Role of amp-activated protein kinase in the control of glucose homeostasis. *Curr. Mol. Med.* **2005**, *5*, 341–348.
32. Yuan, Z.Q.; Li, K.W. Role of farnesoid X receptor in cholestasis. *J. Dig. Dis.* **2016**, *17*, 501–509. [CrossRef] [PubMed]
33. Sammons, M.F.; Price, D.A. Modulation of adipose tissue thermogenesis as a method for increasing energy expenditure. *Bioorganic Med. Chem. Lett.* **2014**, *24*, 425–429. [CrossRef] [PubMed]
34. Lu, T.; Dang, S.; Rui, Z.; Ying, W.; Nie, Z.; Tao, H.; Wei, Z. Adamts18 deficiency promotes colon carcinogene-sis by enhancing β-catenin and p38mapk/erk1/2 signaling in the mouse model of aom/dss-induced coli-tis-associated colorectal cancer. *Oncotarget* **2017**, *8*, 18979–18990. [CrossRef]
35. Volloch, V.; Olsen, B.R. Why cellular stress suppresses adipogenesis in skeletal tissue, but is ineffective in adipose tissue: Control of mesenchymal cell differentiation via integrin binding sites in extracellular matrices. *Matrix Biol.* **2013**, *32*, 365–371. [CrossRef]
36. Suh, J.M.; Gao, X.; McKay, J.; McKay, R.; Salo, Z.; Graff, J.M. Hedgehog signaling plays a conserved role in inhibiting fat formation. *Cell Metab.* **2006**, *3*, 25–34. [CrossRef]
37. Liang, S.; Chen, R.-T.; Zhang, D.-P.; Xin, H.-H.; Lu, Y.; Wang, M.-X.; Miao, Y.-G. Hedgehog signaling pathway regulated the target genes for adipogenesis in silkworm *Bombyx mori*. *Insect Sci.* **2014**, *22*, 587–596. [CrossRef]
38. Yang, Y.; Hsu, P.J.; Chen, Y.S.; Yang, Y.G. Dynamic transcriptomic m6a decoration: Writers, erasers, readers and functions in rna metabolism. *Cell Res.* **2018**, *28*, 616–624. [CrossRef]
39. Wang, Y.; Zheng, Y.; Guo, D.; Zhang, X.; Guo, S.; Hui, T.; Yue, C.; Sun, J.; Bai, Z.; Cai, W.; et al. m6A Methylation Analysis of Differentially Expressed Genes in Skin Tissues of Coarse and Fine Type Liaoning Cashmere Goats. *Front. Genet.* **2020**, *10*, 1–12. [CrossRef]
40. Karsai, A.; Müller, S.; Platz, S.; Hauser, M.-T. Evaluation of a Homemade SYBR® Green I Reaction Mixture for Real-Time PCR Quantification of Gene Expression. *Biotechniques* **2002**, *32*, 790–796. [CrossRef]
41. Chen, S.; Zhou, Y.; Chen, Y.; Gu, J. fastp: An ultra-fast all-in-one FASTQ preprocessor. *Bioinformatics* **2018**, *34*, i884–i890. [CrossRef] [PubMed]
42. Langmead, B.; Salzberg, S.L. Fast gapped-read alignment with Bowtie 2. *Nat. Methods* **2012**, *9*, 357–359. [CrossRef]
43. Stark, R.; Brown, G. Diffbind differential binding analysis of chip-seq peak data. *R Package Version* **2011**, *100*, 3.
44. Ahima, R.S.; Flier, J.S. Adipose tissue as an endocrine organ. *Mol. Cell. Endocrinol.* **2010**, *11*, 327–332.
45. Choe, S.S.; Jin, Y.H.; Hwang, I.J.; Kim, J.I.; Kim, J.B. Adipose tissue remodeling: Its role in energy metabolism and metabolic disorders. *Front. Endocrinol.* **2016**, *7*, 30. [CrossRef]
46. Tao, X.; Chen, J.; Jiang, Y.; Wei, Y.; Chen, Y.; Xu, H.; Zhu, L.; Tang, G.; Li, M.; Jiang, A. Transcriptome-wide n 6 -methyladenosine methylome profiling of porcine muscle and adipose tissues reveals a potential mechanism for transcriptional regulation and differential methylation pattern. *BMC Genom.* **2017**, *18*, 336–349. [CrossRef]
47. Meyer, K.D.; Saletore, Y.; Zumbo, P.; Elemento, O.; Mason, C.E.; Jaffrey, S.R. Comprehensive Analysis of mRNA Methylation Reveals Enrichment in 3′ UTRs and near Stop Codons. *Cell* **2012**, *149*, 1635–1646. [CrossRef]
48. Luo, G.-Z.; MacQueen, A.; Zheng, G.; Duan, H.; Dore, L.C.; Lu, Z.; Liu, J.; Chen, K.; Jia, G.; Bergelson, J.; et al. Unique features of the m6A methylome in Arabidopsis thaliana. *Nat. Commun.* **2014**, *5*, 5630–5647. [CrossRef]
49. Wang, Y.; Zegang, Z.; Dayong, D.; Lang, Z.; Tang, K.; Xie, S. Transcriptome-wide high-throughput deep m(6)a-seq reveals unique differential m(6)a methylation patterns between three organs in *Arabidopsis thaliana*. *Genome Biol.* **2015**, *16*, 272.
50. Bost, F.; Aouadi, M.; Binétruy, L.C.B. The role of mapks in adipocyte differentiation and obesity. *Biochimie* **2005**, *87*, 51–56. [CrossRef]
51. Shen, J.; Hao, Z.; Wang, J.; Hu, J.; Liu, X.; Li, S.; Ke, N.; Song, Y.; Lu, Y.; Hu, L.; et al. Comparative Transcriptome Profile Analysis of Longissimus dorsi Muscle Tissues from Two Goat Breeds with Different Meat Production Performance Using RNA-Seq. *Front. Genet.* **2021**, *11*, 1–13. [CrossRef] [PubMed]
52. Ba, K.; Yang, X.; Wu, L.; Wei, X.; Fu, N.; Fu, Y.; Lin, Y. Jag-ged-1-mediated activation of notch signalling induces adipogenesis of adipose-derived stem cells. *Cell Prolif.* **2012**, *45*, 538–544. [CrossRef]
53. Gustafson, B.; Smith, U. Cytokines promote wnt signaling and inflammation and impair the normal differentiation and lipid accumulation in 3t3-l1 preadipocytes. *J. Biol. Chem.* **2006**, *281*, 9507–9516. [CrossRef] [PubMed]
54. Go, G.W.; Oh, S.; Park, M.; Gang, G.; Kim, Y. T10,c12 conjugated linoleic acid upregulates hepatic de novo lipogenesis and triglyceride synthesis via mtor pathway activation. *J. Microbiol. Biotechnol.* **2013**, *23*, 1569. [CrossRef] [PubMed]
55. Fu, C.; Zhang, Y.; Yao, Q.; Wei, X.; Shi, T.; Yan, P.; Liu, X. Maternal conjugated linoleic acid alters hepatic lipid metabolism via the AMPK signaling pathway in chick embryos. *Poult. Sci.* **2020**, *99*, 224–234. [CrossRef] [PubMed]
56. Guannv, L.; Meihang, L.; Yatao, X.; Song, W.; Muhammad, S.; Chao, S. Colxv promotes adipocyte differentiation via inhibiting DNA methylation and camp/pka pathway in mice. *Oncotarget* **2019**, *8*, 60135–60148.
57. Han, J.; Yu, X.; Wang, S.; Wang, Y.; Liu, Q.; Xu, H.; Wang, X. Igf2bp2 in-duces u251 glioblastoma cell chemoresistance by inhibiting foxo1-mediated pid1 expression through stabilizing lncrna dancr. *Front. Cell Dev. Biol.* **2022**, *9*, 659228. [CrossRef]
58. Guan, H.; Tan, P.; Xie, L.; Mi, B.; Fang, Z.; Li, J.; Yue, J.; Liao, H.; Li, F. Foxo1 inhibits osteosarcoma oncogenesis via wnt/β-catenin pathway suppression. *Oncogenesis* **2015**, *4*, e166. [CrossRef]
59. Koth, M.L.; Garcia-Moreno, S.A.; Novak, A.; Holthusen, K.A.; Jorgensen, J.S. Canonical wnt/β-catenin activ-ity and differential epigenetic marks direct sexually dimorphic regulation of irx3 and irx5 in developing gonads. *Development* **2020**, *147*, dev. 183814.
60. Schymik, H.D.; Barghash, A.; Kiemer, A.K. The m6a reader igf2bp2 regulates macrophage phenotypic activation and inflammatory diseases by stabilizing tsc1 and pparγ. *Adv. Sci.* **2022**, *8*, 2100209.

61. Chawla, A.; Boisvert, W.A.; Lee, C.H.; Laffitte, B.A.; Tontonoz, P. A ppar gamma-lxr-abca1 pathway in macrophages is involved in cholesterol efflux and atherogenesis. *Mol. Cell* **2001**, *7*, 161–171. [CrossRef] [PubMed]
62. Ji, F.; Chen, S.Y.; Yu, Y.; Lin, X.L.; Zhu, Y.F.; Luo, X. Igf2bp2-modified circular rna circarhgap12 promotes cervical cancer progression by interacting m(6)a/foxm1 manner. *Cell Death Discov.* **2021**, *7*, 215. [CrossRef] [PubMed]
63. Jiang, Y.; Zhang, H.; Li, W.; Yan, Y.; Gu, W. Foxm1-activated linc01094 promotes clear cell renal cell carci-noma development via mir-224-5p/chsy1. *Mol. Cell. Biol.* **2019**, *40*, e00357-19.
64. Zang, C.-S.; Huang, H.-T.; Qiu, J.; Sun, J.; Ge, R.-F.; Jiang, L.-W. MiR-224-5p targets EGR2 to promote the development of papillary thyroid carcinoma. *Eur. Rev. Med. Pharmacol. Sci.* **2020**, *24*, 4890–4900. [PubMed]
65. Groenewoud, M.J.; Dekker, J.M.; Fritsche, A.; Reiling, E.; Nijpels, G.; Heine, R.J.; Maassen, J.A.; Machicao, F.; Schfer, S.A.; Hring, H.U. Variants of cdkal1 and igf2bp2 affect first-phase insulin secretion during hyper-glycaemic clamps. *Diabetologia* **2008**, *51*, 1659–1663. [CrossRef]
66. Coffer, P.J.; Puijenbroek, A.V.; Burgering, B.M.; Jonge, K.D.; Koenderman, L.; Bos, J.L.; Kruijer, W. Insulin activates stat3 independently of p21ras-erk and pi-3k signal transduction. *Oncogene* **1997**, *15*, 2529–2539. [CrossRef]
67. Tang, Y.; Weng, X.; Liu, C.; Li, X.; Chen, C. Hypoxia enhances activity and malignant behaviors of colorectal cancer cells through the stat3/microrna-19a/pten/pi3k/akt axis. *Anal. Cell. Pathol.* **2021**, *2021*, 4132488. [CrossRef]
68. Ye, M.; Hui, C.; Min, L. Mir-19a overexpression contributes to heart failure through targeting adrb1. *Int. J. Clin. Exp. Med.* **2015**, *8*, 642–649.
69. Conejo, R.; Alvaro, C.D.; Benito, M.; Cuadrado, A.; Lorenzo, M. Insulin restores differentiation of ras-transformed c2c12 myoblasts by inducing nf-kappab through an akt/p70s6k/p38-mapk pathway. *Oncogene* **2002**, *21*, 3739–3753. [CrossRef]
70. Xu, B.; Peng, Y.-J.; Zhu, W.-J. Curcumin Inhibits Viability of Clear Cell Renal Cell Carcinoma by Down-Regulating ADAMTS18 Gene Methylation though NF-κ B and AKT Signaling Pathway. *Chin. J. Integr. Med.* **2021**, *28*, 419–424. [CrossRef]
71. Wang, H.; Yang, S.; Yang, E.; Zhu, Z.; Li, K. Nf-κb mediates the transcription of mouse calsarcin-1 gene, but not calsarcin-2, in c2c12 cells. *BMC Mol. Biol.* **2007**, *8*, 19. [CrossRef] [PubMed]
72. Lawrence, T.; Fong, C. The resolution of inflammation: Anti-inflammatory roles for nf-κb—Sciencedirect. *Int. J. Biochem. Cell Biol.* **2010**, *42*, 519–523. [CrossRef] [PubMed]
73. Corvol, H.; Rousselet, N.; Thompson, K.E.; Berdah, L.; Cottin, G.; Foussigniere, T.; Longchampt, E.; Fiette, L.; Sage, E.; Prunier, C.; et al. FAM13A is a modifier gene of cystic fibrosis lung phenotype regulating rhoa activity, actin cytoskeleton dynamics and epithelial-mesenchymal transition. *J. Cyst. Fibros.* **2018**, *17*, 190–203. [CrossRef] [PubMed]
74. Bai, X.; Chen, X.; Liu, Y.; Tian, L.; Zhou, Q.; Liu, S.; Fang, J.; Chen, J. Effects of water extract and crude poly-saccharides from liriope spicata var. Prolifera on insr/irs-1/pi3k pathway and glucose metabolism in mice. *J. Ethnopharmacol.* **2009**, *125*, 482–486. [CrossRef] [PubMed]
75. Qiu, W.; Leibowitz, B.; Zhang, L.; Yu, J. Growth factors protect intestinal stem cells from radiation-induced apoptosis by suppressing PUMA through the PI3K/AKT/p53 axis. *Oncogene* **2009**, *29*, 1622–1632. [CrossRef]
76. Chen, J.; Wang, J.; Li, H.; Wang, S.; Xiang, X.; Zhang, D. p53 activates miR-192-5p to mediate vancomycin induced AKI. *Sci. Rep.* **2016**, *6*, 38868. [CrossRef]
77. Zhang, Y.; Huang, R.; Zhou, W.; Zhao, Q.; Lü, Z. miR-192-5p mediates hypoxia/reoxygenation-induced apoptosis in H9c2 cardiomyocytes via targeting of FABP3. *J. Biochem. Mol. Toxicol.* **2016**, *31*, e21873. [CrossRef]
78. Xu, J.; Jia, L.; Ma, H.; Li, Y.; Ma, Z.; Zhao, Y. Axl gene knockdown inhibits the metastasis properties of hepatocellular carcinoma via pi3k/akt-pak1 signal pathway. *Tumor Biol.* **2013**, *35*, 3809–3817. [CrossRef]
79. Liu, F.; Cheng, Z.; Li, X.; Li, Y.; Zhang, H.; Li, J.; Liu, F.; Xu, H.; Li, F. A novel pak1/atf2/mir-132 signaling axis is involved in the hematogenous metastasis of gastric cancer cells. *Mol. Therapy. Nucleic Acids* **2017**, *8*, 370–382. [CrossRef]
80. Yao, C.; Shi, X.; Zhang, Z.; Zhou, S.; Qian, T.; Wang, Y.; Ding, F.; Gu, X.; Yu, B. Hypoxia-Induced Upregulation of miR-132 Promotes Schwann Cell Migration After Sciatic Nerve Injury by Targeting PRKAG3. *Mol. Neurobiol.* **2015**, *53*, 5129–5139. [CrossRef]
81. Feng, C.; Chen, Y.; Zhang, Y.; Yan, Y.; Yang, M.; Gui, H.; Wang, M. PTEN Regulates Mitochondrial Biogenesis via the AKT/GSK-3β/PGC-1α Pathway in Autism. *Neuroscience* **2021**, *465*, 85–94. [CrossRef] [PubMed]
82. Kawakami, Y.; Tsuda, M.; Takahashi, S.; Taniguchi, N.; Esteban, C.R.; Zemmyo, M.; Furumatsu, T.; Lotz, M.; Belmonte, J.C.I.; Asahara, H. Transcriptional coactivator PGC-1α regulates chondrogenesis via association with Sox9. *Proc. Natl. Acad. Sci. USA* **2005**, *102*, 2414–2419. [CrossRef] [PubMed]
83. Liu, Y.; Wu, H.; Zhang, F.; Yang, J.; He, J. Resveratrol upregulates mir-455-5p to antagonize cisplatin ototoxicity via modulating the pten-pi3k-akt axis. *Biochem. Cell Biol. = Biochim. Biol. Cell.* **2021**, *99*, 385–395. [CrossRef] [PubMed]
84. Chen, W.; Li, Q.; Zhang, G.; Wang, H.; Zhu, Z.; Chen, L. Lncrna hoxa-as3 promotes the malignancy of glio-blastoma through regulating mir-455-5p/usp3 axis. *J. Cell. Mol. Med.* **2020**, *24*, 11755–11767. [CrossRef]
85. Wu, X.; Wang, H.; Zhu, D.; Chai, Y.; Wang, J.; Dai, W.; Liu, S. Usp3 promotes gastric cancer progression and metastasis by deubiquitination-dependent col9a3/col6a5 stabilisation. *Cell Death Dis.* **2022**, *13*, 10. [CrossRef]
86. Zhang, Y.; Zhang, L.; Chu, W.; Wang, B.; Zhang, J.; Zhao, M.; Li, X.; Li, B.; Lu, Y.; Yang, B. Tanshinone iia inhibits mir-1 expression through p38 mapk signal pathway in post-infarction rat cardiomyocytes. *Cell. Physiol. Biochem.* **2009**, *26*, 991–998. [CrossRef]
87. Che, X.; Chen, T.; Wei, L.; Gu, X.; Gao, Y.; Liang, S.; Li, P. Microrna1 regulates the development of osteoarthritis in a col2a1creert2/gfpfl/flrfpmir1mouse model of osteoarthritis through the downregulation of indian hedgehog expression. *Int. J. Mol. Med.* **2020**, *46*, 360–370. [CrossRef]

88. Shimoyama, A.; Wada, M.; Ikeda, F.; Hata, K.; Matsubara, T.; Nifuji, A.; Noda, M.; Amano, K.; Yamaguchi, A.; Nishimura, R.; et al. Ihh/Gli2 Signaling Promotes Osteoblast Differentiation by Regulating Runx2 Expression and Function. *Mol. Biol. Cell* **2007**, *18*, 2411–2418. [CrossRef]
89. Zhu, C.W.L.; Nie, X.Y.; Yang, X.F.; Gao, K.G.; Jiang, Z.Y. Dietary dibutyryl camp supplementation regulates the fat deposition in adipose tissues of finishing pigs via camp/pka pathway. *Anim. Biotechnol.* **2021**, *6*, 1–14. [CrossRef]
90. Yang, A.; Kang, Q.; Zhao, Y.; Hu, X.; Li, N.; Hong, W. Lats2 modulates adipocyte proliferation and differentiation via hippo signaling. *PLoS ONE* **2013**, *8*, e72042.
91. Zhang, Y.; O'Keefe, R.J.; Jonason, J.H. BMP-TAK1 (MAP3K7) Induces Adipocyte Differentiation Through PPARγ Signaling. *J. Cells Biochem.* **2016**, *118*, 204–210. [CrossRef] [PubMed]
92. Zhao, L.; Ha, J.-H.; Okla, M.; Chung, S. Activation of autophagy and AMPK by gamma-tocotrienol suppresses the adipogenesis in human adipose derived stem cells. *Mol. Nutr. Food Res.* **2013**, *58*, 569–579. [CrossRef] [PubMed]

Disclaimer/Publisher's Note: The statements, opinions and data contained in all publications are solely those of the individual author(s) and contributor(s) and not of MDPI and/or the editor(s). MDPI and/or the editor(s) disclaim responsibility for any injury to people or property resulting from any ideas, methods, instructions or products referred to in the content.